NOISE MEASUREMENTS OF A CAVITATING PROPELLER IN DIFFERENT FACILITIES: RESULTS OF THE ROUND-ROBIN TEST PROGRAMME

Giorgio Tani, Department of Electrical, Electronic, Telecommunication Engineering and Naval Architecture, Università degli Studi di Genova (UNIGE), Italy
Michele Viviani, Department of Electrical, Electronic, Telecommunication Engineering and Naval Architecture, Università degli Studi di Genova (UNIGE), Italy
Mario Felli, Istituto di ingegneria del Mare (CNR-INM), Italy
Frans Hendrik Lafeber, Maritime Research Institute Netherlands (MARIN), the Netherlands
Thomas Lloyd, Maritime Research Institute Netherlands (MARIN), the Netherlands
Batuhan Aktas, Fugro Structural Monitoring, UK
Mehmet Atlar, Naval Architecture, Ocean and Marine Engineering, University of Strathclyde (UoS), UK
Hanshin Seol, Korea Research Institute of Ships & Ocean Engineering (KRISO), South Korea
Jan Hallander, SSPA, Sweden
Nobuaki Sakamoto, National Maritime Research Institute (NMRI), Japan

Mitigation of shipping noise is a topical issue in marine engineering because of the dramatic increase in the levels of anthropogenic underwater noise and its impact on marine life. In recent years, hydro-acoustic research has focussed on the development of reliable methods for predicting underwater radiated noise (URN) due to cavitation, which is known to be the dominant contribution to the overall radiated noise spectrum of ships above the cavitation inception threshold. Model-scale measurements are currently considered the most reliable approach to study URN problems in marine engineering and are crucial for the verification and validation of numerical methods. However, their reliability is affected by several uncertainty sources for which suitable test procedures and post-processing techniques are needed.
As a means to better understand the accuracy and reliability of underwater radiated noise measurements, a round-robin (RR) test programme for an open water propeller setup was organized within the Community-of-Practice "Noise" of the HydroTesting Forum, with the aim of comparing results among several institutes (i.e. University of Genova UNIGE, University of Newcastle UNEW, NMRI, SSPA, KRISO, CNR-INM and MARIN). This paper reports an overview of the RR programme and compares the different approaches and results.

1. Introduction

The need for reducing levels of underwater noise in the oceans, particularly in regions where ships and marine life come into proximity, is a topical issue of marine engineering. In this scenario, a major challenge concerns the need to develop and validate reliable noise prediction and assessment tools to support cost-effective evaluation of design about underwater radiated noise (URN), which is expected to become a key element in ensuring a ship's compliance with possible future mandatory regulations.
Model-scale tests are currently the most reliable approach for the prediction of the full-scale URN. Nevertheless, model-scale tests are affected by several uncertainty sources, which, in many cases, can significantly jeopardise their reliability, as pointed out in [1].
A non-exhaustive list includes:

i) the effects of the acoustical response of the facility and reverberation (see, e.g. [2] and [3]),
ii) the influence of facility background noise,
iii) the water quality,
iv) the determination of the loading conditions (i.e. advance ratio or mean thrust coefficient, cavitation number),
v) the correct simulation of the wake field and cavitation inception, influencing cavitation extents and dynamics,
vi) the procedure adopted to scale measured noise spectra to full scale (see [4], [5], [6]),
vii) the influence of instrumentation, measurement procedures and setup.

Within the research community on underwater noise measurements, there is no universally adopted procedure for URN tests at model scale despite similar methods for installation, test condition, data acquisition and scaling being used. The procedure adopted by each facility depends somewhat on the type, size and available range of operating conditions. This scenario has created the need to gain insight into the key aspects influencing the accuracy and reliability of URN measurements at model scale, to evaluate the impact of different experimental facilities and test procedures on full-scale noise predictions. To this end, the Community of Practice (CoP) "Noise" of the HydroTesting Forum (HTF, https://www.hydrotestingforum.org/), which followed from the HydroTesting Alliance (European Network of Excellence), has carried out a round-robin (RR) test programme concerning the URN of a cavitating propeller. The RR test programme involved different propeller scale factors and facility types and dimensions. The present paper reports an overview of the RR programme along with a comparative analysis of the results in terms of cavitation extent and radiated noise.

The paper is organised as follows: the description of the RR test programme is reported in Section 2, together with an overview of the test facilities and the experimental setups. The post-processing procedure employed for noise data is documented in Section 3. The results are discussed in Section 4, focusing on cavitation in sub-section 4.1, and noise in sub-section 4.2. Finally, conclusions are drawn in Section 5.

2. The round-robin test campaign

2.1. Propeller model

The case study selected for the round-robin programme is the five-bladed fixed-pitch propeller model of the research vessel "The Princess Royal". Details of the propeller model and of previous experimental campaigns about this propeller model are reported in [7], [8] and [9].

2.2. Test matrix

Propeller cavitation noise is a complex subject, and many scale effects and measurement issues influence the results of model-scale experiments. In order to focus on the comparison between different facilities, a simple open water configuration was adopted. An arrangement with an inclined shaft was also included to address non-stationary cavitation induced by oblique propeller inflow. In the present paper, only results of tests with the straight shaft configuration are reported and analysed.
For both shaft configurations (straight and inclined shaft), six operational conditions were considered. These conditions are defined as different combinations of advance ratio J and cavitation number σ_V, as given in Table 1, where:

$$J = \frac{V}{(nD)} \tag{1}$$

and

$$\sigma_V = \frac{P_0 + \rho g h - P_V}{0.5 \rho V^2} \quad , \tag{2}$$

where V is the forward speed, n and D are the propeller rotation rate and diameter, ρ is the water density, g is the acceleration due to gravity, h is the water head measured from the centre of the propeller disk, P_0 and P_V are the undisturbed pressure and vapour pressure respectively.

Table 1 – Propeller operational conditions for the round-robin programme, straight shaft configuration.

Loading Condition	**J [-]**	**σ_V [-]**
C1	0.4	13.9
C2		8.1
C3		4.5
C4	0.5	13.9
C5		8.1
C6		4.5

2.3. Facilities and testing procedures

The results of the round-robin tests are influenced by a variety of effects, which are summarized hereafter according to the following categories:

- *Facilities.* The round-robin programme includes three major categories of testing facilities: cavitation tunnels of small (UNIGE, NMRI, UNEW) and large size (KRISO, SSPA), a free-surface cavitation channel (INM) and a depressurised wave basin (MARIN). The main characteristics of the facilities are described in [1].

- *Cavitation testing procedures.* Three propeller diameters and different combinations of flow and propeller rotational speed have been adopted, resulting in Reynolds number (Eq. 3) values ranging from a minimum of 1.11E+06 to a maximum of 2.32E+06.

$$Re_{0.7} = \frac{C_{0.7}\sqrt{V^2 + (0.7\pi nD)^2}}{\nu} \tag{3}$$

  where $C_{0.7}$ is the blade chord length at 0.7R, R being the propeller radius, and ν is the kinematic viscosity of the fluid. These differences implied the adoption of special procedures for cavitation testing in some facilities, to stimulate the transition to turbulent flow. More specifically, MARIN applied strips of carborundum grains on the leading edges of the propeller blades and SSPA used a special paint to increase the surface roughness. Tests were undertaken at thrust coefficient identity, i.e. $K_T = 0.242$ and $K_T = 0.190$, corresponding to $J = 0.4$ and $J = 0.5$ respectively, as derived from towing tank measurements. This approach was adopted by all the participants with the exception of SSPA and KRISO, who performed the tests at J identity, resulting in slightly higher propeller thrust. The operational conditions tested by each participant are described in terms of thrust coefficient K_T and cavitation number based on the propeller tip tangential speed σ_n in Table 2, where:

$$K_T = \frac{T}{\rho n^2 D^4} \quad (4)$$

and

$$\sigma_n = \sigma_V J^2 \quad (5)$$

where T is propeller thrust.

Table 2 – Values of propeller thrust coefficient and cavitation number within the round-robin campaign, straight shaft configuration.

	K_T						σ_n					
Condition	**MARIN**	**UNIGE**	**SSPA**	**UNEW**	**KRISO**	**NMRI**	**MARIN**	**UNIGE**	**SSPA**	**UNEW**	**KRISO**	**NMRI**
C1	0.223	0.244	0.26	0.242	0.255	0.243	2.57	2.223	2.34	2.22	2.14	3.081
C2	0.243	0.244	0.262	0.242	0.255	0.243	1.296	1.311	1.41	1.30	1.30	1.442
C3	0.222	0.226	0.263	0.242	0.255	0.243	0.72	0.721	0.79	0.72	1.13	0.801
C4	0.192	0.190	0.203	0.190	0.203	0.191	3.475	3.486	3.63	3.48	3.32	2.978
C5	0.193	0.189	0.204	0.190	0.203	0.191	2.025	2.024	2.13	2.03	2.03	2.173
C6	0.195	0.191	0.206	0.190	0.203	0.191	1.125	1.137	1.18	1.13	1.12	1.207

- *Water quality*. Water quality accounts for the amount and size of cavitation nuclei that significantly influence cavitation inception and development and thus radiated noise [10]. Also, the amount of dissolved gas may have a relevant effect on the bubble dynamics and collapse, thus influencing the high-frequency noise and acoustic wave propagation [5]. For the round-robin programme, all the participants assessed water quality, measuring the amount of oxygen content (UNIGE, UNEW, NMRI, KRISO) or the total gas content (MARIN, SSPA). Water quality parameters are summarised in Table 3.

Table 3 – Measurements of water quality.

MARIN	Air content at 39% saturation: 10.7 ppm; estimated subdivision in nitrogen (N_2) and oxygen (O_2) (other gases are neglected): N_2: 6.7 ppm, O_2: 4.1 ppm
UNIGE	Oxygen content O_2: 6.2 ppm for the loading condition C4; 3.7 ppm for conditions C3 and C6; 5 ppm for the remaining conditions
SSPA	Total gas content 20%
UNEW	Oxygen content O_2: between 3.7 and 4 ppm
KRISO	Oxygen content O_2: 6.3 ppm
NMRI	Oxygen content O_2: between 3.7 and 4 ppm

- *Hydrophone configurations.* URN tests were performed using different hydrophone configurations according to facility characteristics and best-related experience. Hydrophones mounted on streamlined supports or fins inside the test section were used by SSPA and NMRI. KRISO and UNEW placed hydrophones in acoustic water-filled chambers of different sizes and characteristics: a large anechoic chamber at KRISO and a small steel cylinder at UNEW. UNIGE adopted a multi-hydrophone configuration using two streamlined fins and one small acrylic glass chamber. A different configuration was used in the depressurised wave basin of MARIN, consisting of one hydrophone mounted on a mast raised from the bottom of the tank at 1.45 m below the free surface. MARIN's arrangement was the only one in which the propeller and the hydrophone were in relative motion.

- *Propeller arrangement.* Propeller vortex dynamics is strongly influenced whether pushing or pulling configuration is adopted, particularly for drift conditions [11]. This influence is supposed to affect the URN. In order to minimise any uncertainty due to the adoption of different propeller arrangements, it was decided to undertake all the tests with the propeller in pulling operation.

- *Confined environment effects.* URN propagation is significantly affected by facility size and characteristics. This effect can be addressed by the use of transfer functions accounting for the facility specificity in the acoustic wave propagation. For the present round-robin programme, only three institutions adopted solutions to accounting for confined environment effects: UNIGE and SSPA measured the transfer function following the ITTC guidelines [12] whereas MARIN computed the Lloyd's Mirror effect using the method presented in [13], free-surface reflections being the major effect on noise propagation in the wave basin since noise is measured within the reverberation radius [14].

3. Post-processing of noise data

Noise signals were acquired according to the standard procedure of each facility concerning the equipment used, the sampling frequency and the acquisition time.
Noise records have been processed to obtain noise spectra in both narrowband and one-third octave (OTO) band representation. To this end, most participants employed methods based on the Fast Fourier Transform (FFT), each with its own choice of window type, length and overlaps. Only UNEW directly acquired the signal in one-third octave band using hardware filters.

The sound pressure levels (SPL) are defined as follows:

$$SPL = 10\log_{10}\left(\bar{p}_{rms}^2/p_{ref}^2\right) \tag{6}$$

where $\bar{p}_{rms}$ is the root mean square of the sound pressure $p(t)$, and p_{ref}= 1 μPa for underwater noise.
In order to identify the contribution of the cavitating propeller, background noise correction is applied. The background noise has been measured by all the participants, replacing the propeller with a dummy hub and running the facility at the same advance speed, shaft rate and depressurisation level adopted for the tests with the propeller. Net noise levels are computed based on the signal-to-noise ratio (SNR), which is the difference between the total sound pressure levels (SPL_{s+n}) and the background sound pressure levels (SPL_n):

SNR ≥ 10 dB: No correction

$$SPL_s = SPL_{s+n} \tag{7}$$

3 dB ≤ *SNR* < 10 dB:

$$SPL_s = 10\log_{10}\left(10^{(SPL_{s+n}/10)} - 10^{(SPL_n/10)}\right) \tag{8}$$

SNR< 3 dB: results are discarted.

The obtained net noise levels SPL_s are scaled to a reference distance using a spherical propagation correction, which leads to Radiated Noise Levels (RNL) as follows:

$$RNL = SPL_s + 20\log_{10}(r/r_{ref}) \tag{9}$$

where r is the distance between the hydrophone and the propeller, r_{ref} is the reference distance, typically equal to 1 m. Alternatively, distance normalization is implicitly accounted for using the transfer function (TF) to derive the Source Strength Levels (SL):

$$SL = SPL_s - TF \tag{10}$$

3.1. Extrapolation to full scale

In order to compare all the results of the round-robin campaign, noise spectra are scaled to a common condition, as specified below:

D_s = 0.75 m
n_s= 19.025 rps
σ_{ns} = 1.06

where D_s is the diameter of the full-scale propeller and n_s and σ_{ns} are the propeller rotational speed and the cavitation number corresponding to the maximum speed of ‘‘The Princess Royal’’. Full-scale noise spectra are obtained according to the ITTC formulation [12]:

$$\frac{\mathrm{f}_s}{\mathrm{f}_m} = \left(\frac{n_s}{n_m}\right)\sqrt{\frac{\sigma_s}{\sigma_m}} \tag{11}$$

$$SPL_s = SPL_m + 20\log_{10}\left[\left(\frac{\sigma_s}{\sigma_m}\right)^w\left(\frac{r_m}{r_s}\right)^x\left(\frac{n_s D_s}{n_m D_m}\right)^y\left(\frac{D_s}{D_m}\right)^z\right] \tag{12}$$

In the above formulas, the subscript s stands for ship and m for the model. The set of exponents corresponding to the low-frequency formulation is used ($w = 0.75,\ x = 1,\ y = 1.5,\ z = 1.5$ for constant bandwidth spectra, $w = 1,\ x = 1,\ y = 2,\ z = 1$ for proportional bandwidth spectra; for the latter, if power spectral density levels are needed, the quantity $10\log_{10}(\Delta f)$, where Δf is the bandwidth, must be subtracted).

4. Results

In this section, results of the round-robin programme are analysed focussing at first on cavitation extents, considering some example of available observations. Then in Subsection 4.2, results of noise measurements are analysed in detail.

4.1. Cavitation extents

Before comparing propeller cavitation extents observed by the different participants, cavitation patterns for all the loading conditions are presented for one participant only, to exemplify the typical cavitation patterns. With this aim, the cavitation observed at SSPA is shown in Fig. 1.

From the analysis of reported pictures, it is possible to make general observations about cavitation patterns present for the loading conditions considered in the round-robin programme:

1) Only suction side cavitation is present, consisting of the leading-edge vortex and sheet cavitation.
2) Sorting the operational conditions concerning the increased sheet cavitation extent, the following result is obtained: C4, C5, C1, C6, C2 and C3.
3) Sorting the operational conditions with respect to increasing vortex cavitation extent, the following result is obtained: C4, C3, C5, C1, C6 and C2.
4) Conditions C1, C2, C5 and C6 are characterized by similar cavitation phenomena and dynamics, differing only for the extent of phenomena.
5) Condition C4 is characterised by the presence of a weak tip vortex, very close to inception.
6) Condition C3 is characterised by rather large sheet cavitation, generating cloud cavitation at trailing edge. The cavitating core of the tip vortex is disrupted. In place of it, cloudy vertical structures are present, featuring a somewhat unstable behaviour. A smaller vortex is generated at the trailing edge of the sheet cavity, where the cavity reaches the blade trailing edge.

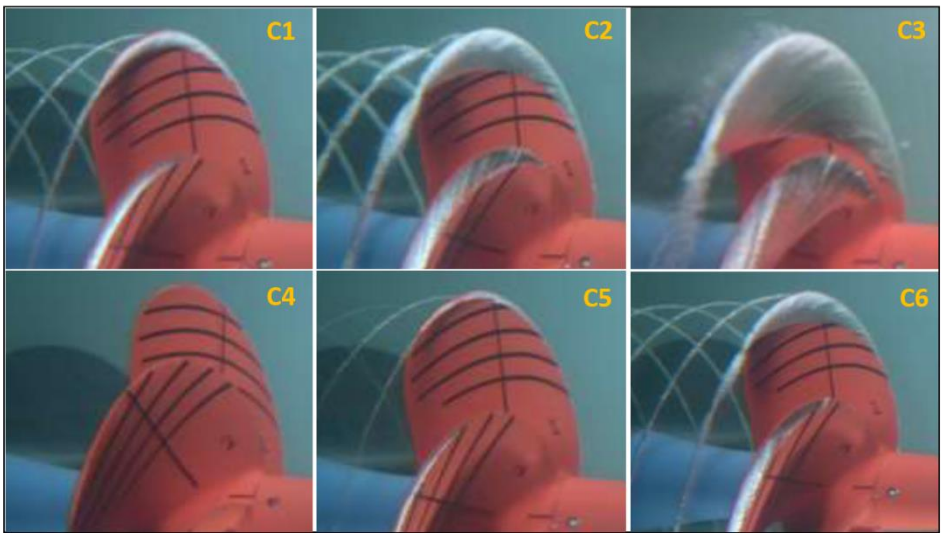

Fig. 1 - Cavitation extents observed at SSPA for all the operational conditions, with the level shaft.

These comments hold for tests carried out by all the participants, with only the following few exceptions:

- The differences between cavitation extents observed at NMRI, for $J = 0.4$ (C1, C2 and C3) and $J = 0.5$ (C4, C5, C6) seem reduced; the tip vortex in condition C4 is more stable than in other institutions, whereas the sheet cavity in condition C3 is reduced. The reasons for these discrepancies may lie in the cavitation numbers adopted for tests, which are slightly different from the nominal values (see Table 2).

- Sheet cavitation observed at KRISO for condition C3 is less extended than that observed by other participants, while the tip vortex is larger. The reason for this is that it was not possible to achieve the very low cavitation number of condition C3 at KRISO using the setup adopted. Hence C3 condition at KRISO is characterised by a higher (about 50%) cavitation number (see Table 2).

The direct comparison of cavitation patterns observed within the round-robin programme is shown in Fig. 2, Fig. 3 and Fig. 4, for conditions C1, C3 and C4, respectively.

A fair agreement is observed in most cases, besides the anomalies already mentioned. Differences for conditions C1 and C3 mainly concern the extent of the sheet cavitation toward the inner radii: sheet cavitation for condition C1 starts around 0.7R for MARIN, UNEW and SSPA, around 0.75R for KRISO, and 0.8 for UNIGE and NMRI; for condition C3 it begins at about 0.3R for MARIN and SSPA, 0.6R for UNEW and UNIGE, 0.65 for KRISO and 0.8 for NMRI.

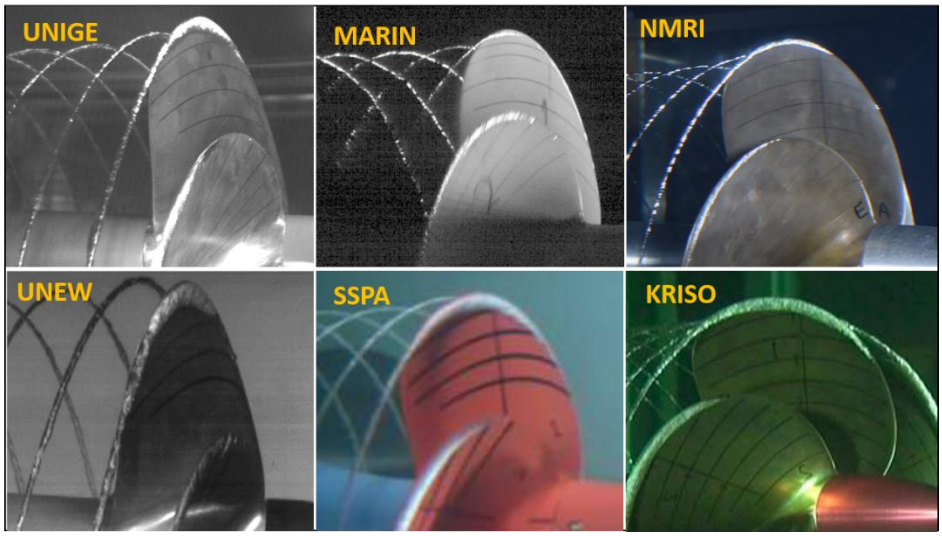

Fig. 2 – Cavitation observed for condition C1 (J=0.4, σ_V=13.9).

Analysing differences in terms of chordwise elongation and thickness of sheet cavitation is even more difficult because of differences in the observation angles. Generally, the chordwise extent of cavitation for condition C1 is approximately 10 % of the chord at inner radii, reaching 100% of the chord around 0.95R. Considering instead condition C3, the radial position where the sheet cavity reaches the trailing edge can be compared: this occurs at about 0.65R for MARIN and SSPA, 0.7R for UNIGE and UNEW, and 0.85R for KRISO and NMRI.

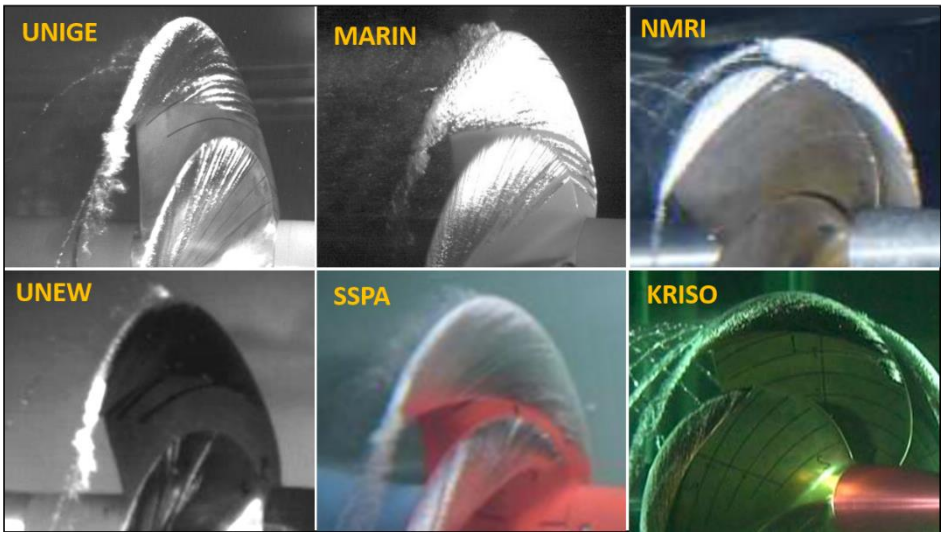

Fig. 3 – Cavitation observed for condition C3 (J=0.4, σ_V=4.5).

Finally, considering condition C4, a very small tip vortex is visible in the UNIGE, MARIN and UNEW observations. Similar cavitation was also present at SSPA and KRISO, even if it was not captured in

photographs because of its intermittent nature. The largest extent of tip vortex at NMRI for this condition is due to the different cavitation number adopted.

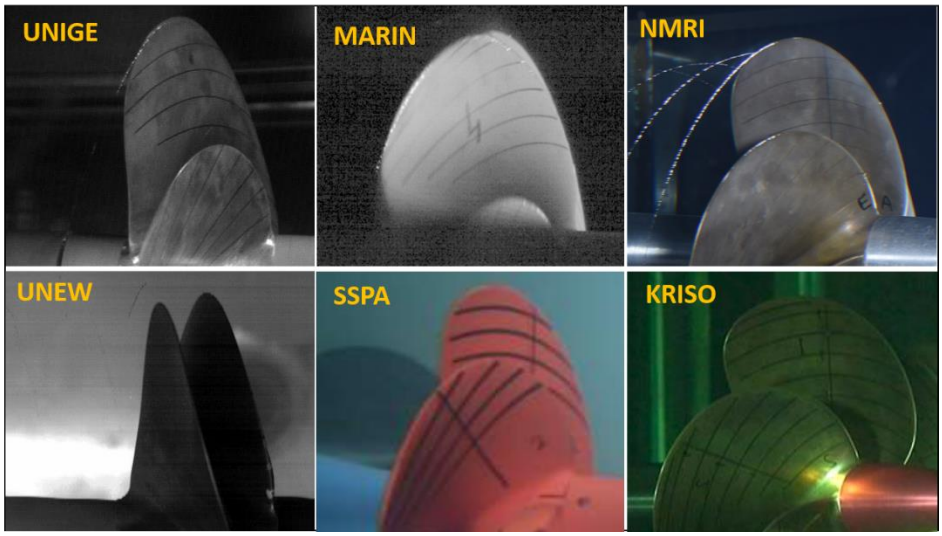

Fig. 4 – Cavitation observed for condition C4 (J=0.5, σ_V=13.9).

From this qualitative analysis it can be concluded that:

- The cavitation observed by the participants is very similar in terms of typology and dynamics, with only a few exceptions for the condition with the most cavitation (C3).
- Differences in terms of the extent of the sheet cavity are small, but non-negligible, for most conditions. The largest differences are observed for the condition with the most cavitation (C3).
- Discrepancies mostly concern the extent of the sheet cavity at the inner radii.

As already remarked, the largest discrepancies observed may be ascribed to the small differences in the operational conditions used between the various facilities for certain tests (mainly in terms of cavitation number). Further differences, especially those concerning the extent of sheet cavitation at inner propeller radii, are likely related to the development of the boundary layer on the blades, which may vary depending on the Reynolds number adopted during tests, as well as on the approach used for turbulence stimulation if applied.

4.2. Radiated noise

The main results of the round-robin programme are comparisons of noise measurements carried out by the different participants. The comparison of noise spectra is reported in Fig. 5. These full-scale spectra are obtained by scaling all the measurements according to the procedure described in Section 3.
Some anomalous peaks are present in the spectra, caused by the presence of significant tonal noise disturbances not cancelled by the background noise correction (e.g. propeller singing, structural vibrations, shaft line noise).
Disregarding the frequency bands containing peaks, a band of variation of about 10 dB of predicted noise levels is observed on average, rising to about 20 dB for conditions C3 and C4.

Results of this overall comparison depend on the considered frequency range:

- High-frequency noise (above 2 - 3 kHz): higher levels have been measured at SSPA and KRISO, while the lowest levels are in most cases those measured at UNIGE and MARIN.
- Low-frequency noise (below 2 - 3 kHz): higher noise levels have been measured at SSPA, UNIGE and, for some conditions, NMRI and KRISO. The agreement in this frequency range is slightly better, even if there are always some spectra deviating from the most common behaviour.

For most of the conditions tested, similarities between the results obtained by the different participants can be observed. However, the spread of measured noise levels is quite large and requires further investigation.

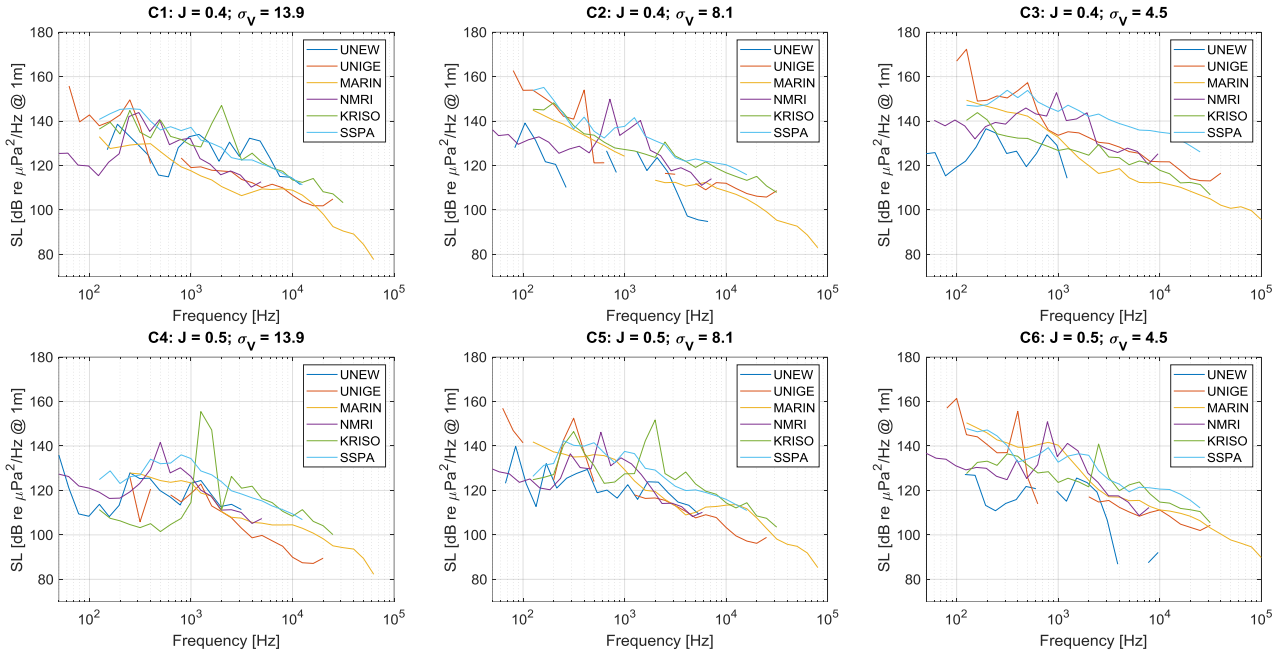

Fig. 5 – Comparison of predicted full-scale source levels for all six conditions measured.

Noise spectra are characterised by complex shapes, with many features that are not always directly related to the physics of the noise source analysed. These include the tonal noise disturbances already mentioned, as well as different background noise in terms of a continuous spectrum, propagation effects, and possible noise absorption caused by free bubbles, amongst others. Nevertheless, comparing most of the spectra with the theoretical spectra of cavitation noise (see for example [5], [15] and [16]), some common features may be observed. In many cases, the continuous part of the cavitation noise spectrum is characterised by the presence of a hump at a medium-low frequency, whose amplitude and prominence depend on cavitation typology and dynamics. This hump usually represents the peak in the broadband spectrum.

Moving to higher frequencies, noise levels vary with a certain constant power of the reciprocal of the frequency. In some cases, two different frequency ranges may be observed, with different decay ratios. The decay slope typically increases with increasing frequency.

It is possible to identify the main features of this theoretical cavitation noise spectra, as illustrated in Fig. 6. The analysis of the main characteristics of this schematic spectrum may provide a more in-depth insight into the physics of the problem. The features that are more directly related to the dynamics of cavitation are the central frequency, amplitude, width and power content of the spectral hump; and the

energy content and decay ratio of the high-frequency part of the spectrum. The hump is associated with low-frequency dynamics of cavities, such as the pulsation of the tip vortex [17] or the growth and initial stage of the collapse of cavities [16]. The high-frequency spectrum and its characteristics are instead associated with the dynamics, and the size of small cavitation bubbles shed by cavitation, with the final stage of cavity collapse and with the generation of shock waves.

From a practical point of view, a schematic representation based on piecewise linear functions, as shown in the example in Fig. 6, is used to define the main characteristics of spectra for further analyses.

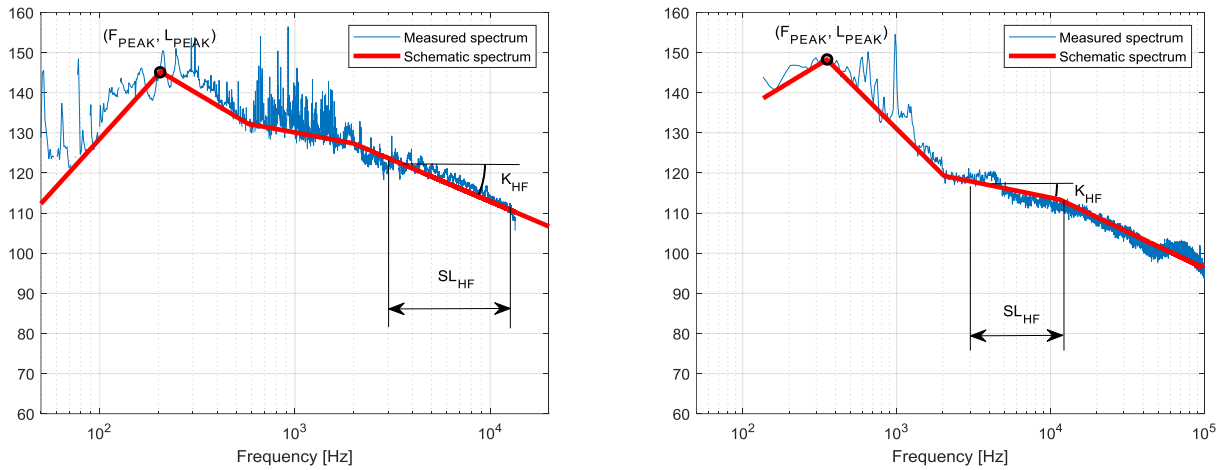

Fig. 6 – Possible schematization of the cavitation noise spectrum.

In this work, the analysis is focused on the following parameters:

- F_{PEAK} and SL_{PEAK}: frequency and level of the peak in the schematic spectrum.
- K_{HF}: decay ratio of the spectrum computed at 10 kHz.
- SL_{HF}: power content between 3 kHz and 12.5 kHz (computed from the real spectrum).

Keeping in mind the approximations concerning the definition and fitting of the schematic spectrum onto the real spectra, these parameters are analysed in Fig. 7 and Fig. 8, which are dedicated to the hump and the high-frequency spectrum respectively. Results from UNEW are not included in present analysis because of the complex shape of spectra measured in this facility and because narrowband spectra, which allow identifying the characteristics analysed, are not available.

Starting with the hump characteristics, these may be reasonably associated with vortex dynamics for present cases. Actually, when significant tip vortex cavitation is present, without major collapses, as in the round-robin programme, the volume pulsation of the vortex around the natural frequency may characterise the radiated noise spectrum producing the prominent peaks observed in current measurements.

The resonance frequency of a cavitating vortex may be analysed considering the dispersion relation for waves travelling on the cavity surfaces. This relation, under some hypotheses on the deformation mode generating noise, may also provide a relationship between the resonance frequency of the vortex cavity and its dimensions, see [18], [19] and [20]. Accordingly, the analysis of the hump central frequency may provide interesting information on the size of tip vortex cavitation.

Values reported on the left side of Fig. 8, show a rather good agreement between UNIGE, MARIN, KRISO and SSPA, while the trend observed at NMRI is completely different. The anomalous behaviour of the hump in NMRI spectra may be due to the fact that the identified hump is probably not related to tip vortex noise, whereas the spectral hump corresponding to vortex pulsation is not clearly detectable. This conclusion is confirmed by the analysis of the peak levels and other characteristics of the hump (e.g. the width), which present similar anomalous trends.

Focussing on the remaining measurements, the following main comments may be made:

- Considering $J = 0.4$ (C1, C2 and C3), the hump centre frequency decreases from C1 to C2, where the minimum is observed, while it increases for condition C3. This trend is consistent with cavitation extents, since the dimensions of the cavitating vortices increase from C1 to C2, where the largest vortices are observed. For condition C3 the main vortex is disrupted while a second weaker vortex is present, causing the hump at increased frequency with respect to C1 and C2. Condition C3 at KRISO has been reproduced with a slightly higher cavitation number, causing a different cavitation extent and dynamics, as already discussed in Section 4.1. The resulting vortex exhibits a cavitating core slightly larger than that of condition C2, without any secondary vortex. This agrees rather well with the decrease of the hump frequency from condition C2 to C3 observed at KRISO.
- Focussing on $J = 0.5$ (C4, C5 and C6), the maximum hump frequency is observed in correspondence to condition C4, which is consistent with the very small dimensions of the tip vortex for this condition. Moving to conditions C5 and C6, the hump frequency decreases again, which is in good agreement with the increasing cavitating radius.
- Sorting the central frequency values for a given participant, in decreasing order, the result agrees with the tip vortex dimensions qualitatively observed in Section 4.1.

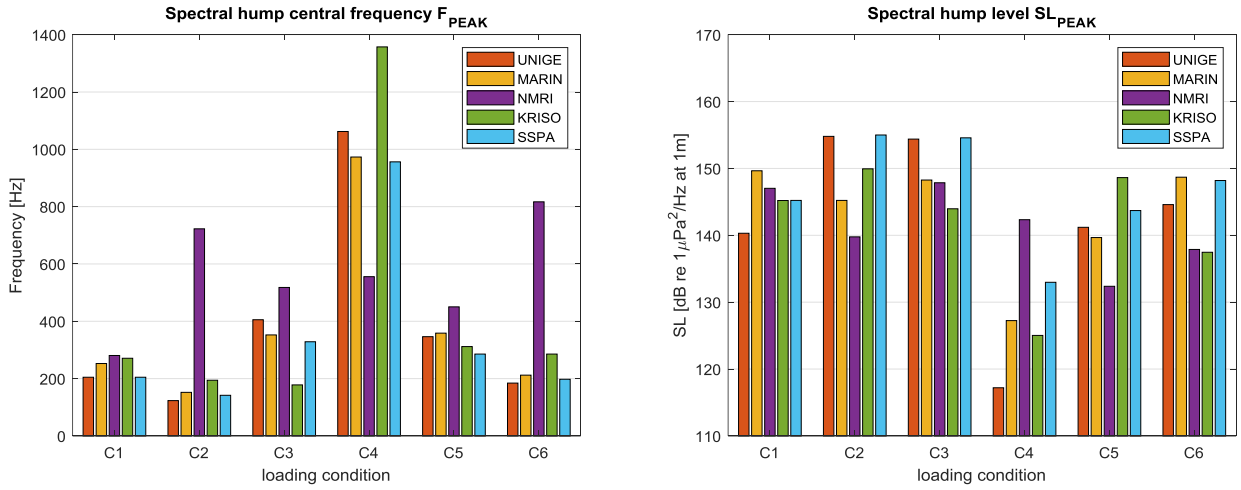

Fig. 7 – Main characteristics of cavitation noise spectra: (left) centre frequency of the spectral hump (right) peak level of the spectral hump.

Based on these observations, and in as far as the peak frequency may be considered representative of the vortex pulsation frequency, the agreement observed in terms of vortex dynamics is significantly better than that inferable from the overall comparison of noise spectra. Actually, in most cases the range of

variation is below 100 Hz with a few exceptions observed in the measurements performed at KRISO, which are most probably due to the small differences in the operational conditions as already remarked. Moving to the analysis of the peak levels, the comparison is more complicated, and the agreement within participants' results is relatively worse; nevertheless, common trends are present:

- Minimum levels are observed for condition C4, for which the vortex is just past inception.
- Noise levels increase significantly from condition C4 to C5 and C6, except for C6 at KRISO and NMRI, whose hump interpretation is doubtful, as already remarked.
- The trend is more complicated considering conditions with $J = 0.4$, and lower differences are observed between conditions C1, C2 and C3 than between C4, C5 and C6 ($J = 0.5$).
- Sorting the peak levels, for a given participant, in increasing order, the results are different depending on the selected participant, and generally, it is more difficult to correlate the obtained order with that of vortex dimensions.
- The spread in results is in most cases of about 10 dB, except for condition C4, which shows larger variation due to incipient and intermittent cavitation. This general value is significant, but probably lower than the overall spread observed from the global analysis of the spectra.

In summary, the interpretation of peak levels is more complex than peak frequency, with a far less good agreement between the different institutes found. The identification of the spectral hump may not be correct in some cases, or its interpretation as the noise associated with tip vortex pulsation may be not completely correct or consistent. On the other hand, differences in noise levels may be not caused only by differences in the noise sources, and may be partially related to other effects such as the acoustic response of the facility, sensors, etc.

The high-frequency spectrum is mainly related to the collapse of cavities. For uniform inflow conditions, the main cavities show an almost stationary behaviour, hence collapses mainly concern the small cavities shed from both sheet cavitation and tip vortex cavitation. Therefore, the intensity and frequency content of the high-frequency noise should depend on the amount, frequency and intensity of collapses, which are related to cavitation extents and other aspects influencing bubble dynamics, such as the presence of non-condensable gas and fluid compressibility.

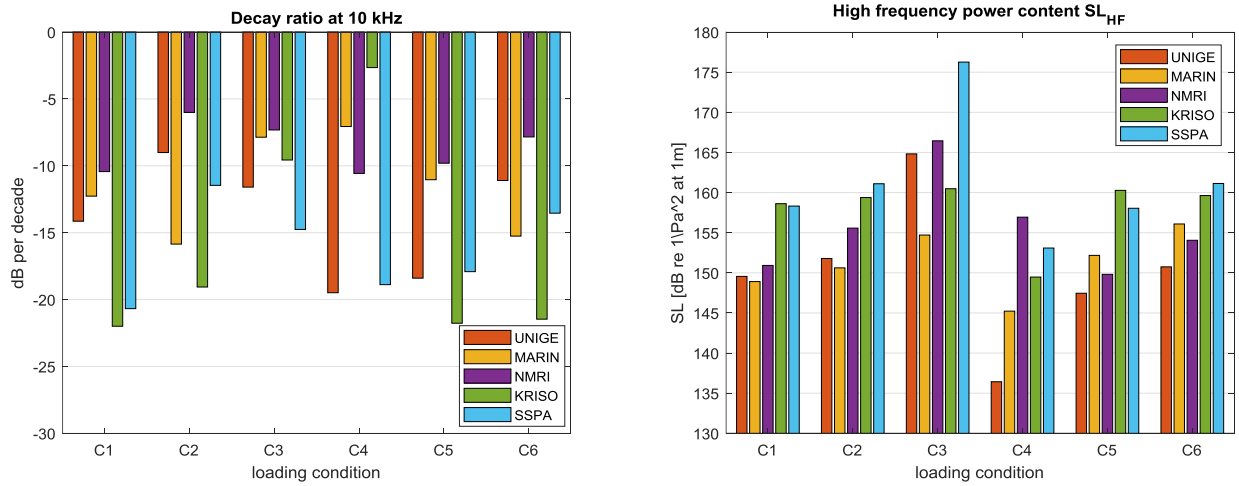

Fig. 8 – Main characteristics of cavitation noise spectra: (left) decay ratio of the high frequency spectrum; (right) power content of the high-frequency spectrum.

Analysing the average decay ratio of the high-frequency spectrum, reported on the left side plot of Fig. 8, a significant spread of results is observed. Most values are between -10 and -20 dB per decade, in good agreement with data on cavitation noise available in the literature [21]. The reasons for the spread in the data within different participants and operational conditions are not clearly understood. The analysis of the decay ratio at a given frequency allows comparing the characteristics of the high frequency noise spectrum only partially. As clearly visible in the examples shown in Fig. 6, this frequency (i.e. 10 kHz) is otherwise lower or higher than the frequency that divides the two spectral parts with different decay slopes of the schematized spectrum.

Finally, the right plot in Fig. 8 reports the sound pressure level computed over a wide frequency range, defined in such a way as to represent the power content of the high-frequency spectrum for all the participants. The spread of values is significant: differences of 10 dB on average are observed for the condition with intermediate cavitation (C1, C2, C5 and C6) while even 20 dB differences are observed between the highest and lowest levels for conditions C3 and C4. The latter conditions, being characterized by very large cavitation and incipient cavitation respectively, are relatively more sensitive to possible differences between experiments carried out by the participants; therefore, it is not completely surprising to observe a larger spread of results for such conditions. However, the magnitude of the spread of data, for both intermediate and extreme cavitation cases, is larger than desired.

Focussing instead on the trends concerning propeller loading conditions, some similarities are detectable, with only a few exceptions. The main common features are:

- The high-frequency noise increases from condition C1 to C3 and from C4 to C6.
- The high-frequency noise is higher for $J = 0.4$, for which more (sheet) cavitation is present compared to $J = 0.5$.
- Maximum and minimum noise levels are measured for condition C3 and C4, respectively (except NMRI), which is in good agreement with the observed cavitation patterns.
- Sorting the high-frequency noise levels, for a given participant, in increasing order, the results partially agree with the sheet cavitation extent. In most cases, noise levels for the intermediate cavitation conditions (C1, C2, C5 and C6) are rather similar.

The analyses presented, focussing on noise levels for a single frequency band or on the level of the peak - as in Fig. 7 - allows appreciation of how noise levels vary with respect to propeller loading conditions for each participant. It can be concluded that differences in noise levels found by each participant when modifying propeller loading conditions (at least, limited to intermediate cavitation conditions (C1, C2, C5 and C6)) are comparable, and in many cases lower than differences present between results obtained by the different participants for the same propeller loading condition.

5. Conclusions

Results of the round-robin campaign on propeller noise measurements at model scale, carried out by The Noise Community of Practice of the HydroTesting Forum, are analysed. The comparison of available data provides interesting information on cavitation model testing and noise measurement. Cavitation patterns observed within the round-robin programme are generally very similar in terms of phenomena, extent and dynamics. Several discrepancies do exist, however. Many reasons may contribute to these differences, among which the most important are the small differences in the definition of the operational

conditions and the development of the boundary layer on propeller blades. Also, possible differences in the geometry of propeller models could play a role and should be analysed in the future.

The analysis of noise results highlighted the significant spread of data, even when trying to neglect the effects of unwanted noise components. Some important comments may be made based on the analysis of the main characteristics of the noise spectra, namely the frequency and the peak level of the medium-low frequency hump, and the decay ratio and power content of the high-frequency noise:

- Common trends have been observed for all the considered characteristics.
- A rather good agreement is present in terms of the centre frequency of the spectral hump, which is most highly associated with the noise generated by tip vortex cavitation. The values of the frequencies correlate rather well also with observed extents of vortex cavitation.
- The peak levels of the medium-low frequency hump present a significant spread instead. Even if the dependency of this quantity on propeller loading showed some similarities for each participant, discrepancies are present, and it is more difficult to recognise a common trend.
- The decay slope of the high-frequency spectrum is rather different for each participant, although most values lay within values reported in the literature for cavitation noise. However, due to the different frequency range available for each participant, it is difficult to compare the features of high-frequency noise more deeply.
- The power content of the high-frequency noise is characterised by a significant spread, even if some common trends are observed in terms of dependency of the noise levels on propeller loading conditions.
- Differences observed in terms of noise levels comparing all the propeller loading conditions characterised by moderate cavitation, for a given participant, are comparable or even lower than differences observed comparing measurements carried out by all the participants for a given loading condition.

In summary, the comparison of results obtained within the round-robin programme highlights the need for further studies, since such large discrepancies should be explained. In view of this, the analyses reported here already provide some useful indications.

Some differences between the experiments carried out by the participants of the round-robin programme also exist in terms of the definition of propeller loading conditions and cavitation extents. However, these differences are not expected to cause the large discrepancies that are observed between noise data. Observed cavitation is always characterised by the same dynamic behaviour and similar extents; also, the analysis of the central frequency of the spectral hump suggests that vortex dynamics are similar for most of the participants. Finally, the overall analysis of the effects of the loading conditions on measured noise confirms that these effects are not sufficient to explain the large dispersion of data.

Based on these conclusions, further aspects will be investigated in the future, not only concerning the development of cavitation but also the generation, propagation, acquisition and processing of noise data, including the following main aspects:

- Effects of water quality on noise generation and propagation.
- Effects of the acoustic response of the facility.
- Effects of the oblique flow.
- Effects of the adoption of different scaling laws to compare results of the round-robin campaign.

Also, further tests will be carried out within the round-robin programme, namely at the CNR-INM free-surface cavitation channel. These further tests will provide a valuable opportunity to carry out additional investigations to clarify some of the observed issues.

References

1. Tani, G., Viviani, M., Felli, M., Lafeber, F. H., Lloyd, T., Aktas, B., Atlar, M., Seol, H., Hallander, J., Sakamoto, N., Kamiirisa, H., (2019), "Round Robin Test on Radiated Noise of a Cavitating Propeller", Sixth International Symposium on Marine Propulsors smp'19, Rome, Italy, May 2019.
2. Briancon, L., Fournier, P., Fréchou, D., (2013), "Marine Propeller Noise Measurements Techniques in Hydroacoustics Tunnel", Symposium on Advanced Measurement Techniques, AMT'13, Gdansk, Poland.
3. Tani, G., Viviani, M., Ferrando, M., Armelloni, E., (2019), "Aspects of the measurement of the acoustic transfer function in a cavitation tunnel.", Applied Ocean Research, Volume 87, Pages 264-278, ISSN 0141-1187, https://doi.org/10.1016/j.apor.2019.02.017.
4. Bark, G., "Prediction of propeller cavitation noise from model tests and its comparison with full scale data", Journal of Fluids Engineering, Vol. 107, pp 112-119, 1985.
5. Blake, W. K., Sevik, M. M., (1982) "Recent developments in cavitation noise research." ASME International Symposium on Cavitation Noise, Phoenix, USA.
6. Lövik, A., (1981) "Scaling of propeller cavitation noise," in Noise sources in ships, Stockholm, Sweden: Nordforsk, 1981.
7. Aktas, B., Atlar, M., Turkmen, S., Shi, W., Sampson, R., Korkut, E., Fitzsimmons, P., (2016), "Propeller cavitation noise investigations of a research vessel using medium size cavitation tunnel tests and full-scale trials." Ocean Eng. 120, 122–135. https://doi.org/10.1016/j.oceaneng.2015.12.040.
8. Lafeber, F.H., Bosschers, J., (2016), "Validation of computational and experimental prediction methods for the underwater radiated noise of a small research vessel." In: Proceedings of PRADS 2016, Copenhagen, Denmark.
9. Tani, G., Aktas, B., Viviani, M., Yilmaz, N., Miglianti, F., Ferrando, M., Atlar, M., (2019) "Cavitation tunnel tests for "The Princess Royal" model propeller behind a 2-dimensional wake screen", Ocean Engineering, Volume 172, Pages 829-843, ISSN 0029-8018, https://doi.org/10.1016/j.oceaneng.2018.11.017.
10. Korkut, E. 1999 An investigation into the scale effects on cavitation inception and noise in marine propellers. PhD thesis, University of Newcastle upon Tyne, UK.
11. Felli, M., & Falchi, M. (2018), "Propeller wake evolution mechanisms in oblique flow conditions." Journal of Fluid Mechanics, 845, 520-559. doi:10.1017/jfm.2018.232
12. ITTC Specialist Committee on Hydrodynamic Noise, (2017) "Model-scale propeller cavitation noise measurements." In: Recommended Procedures and Guidelines 7.5-02-01-05 International Towing Tank Conference.

13. Ainslie, M., (2010), “Principles of sonar performance modelling.” Springer Praxis, Berlin/Heidelberg, doi: 10.1007/978-3-540-87662-5.
14. Lafeber, F.H., Bosschers, J., de Jong, C., Graafland, F., (2015), “Acoustic reverberation measurements in the depressurized towing tank”, 4th International Conference on Advanced Model Measurement Technologies for the Maritime Industry AMT’15, Istanbul, Turkey.
15. Blake, W. K. (1986), “Mechanics of flow-induced sound and vibration.” Academic Press Inc.
16. Fitzpatrick, H. M., Strasberg, M., (1956), “Hydrodynamic sources of sound.” Proc. 1st Symp. On Naval Hydrodynamics, Washington D.C. 241-280. National Academy Press.
17. Terwisga, T., Van Wijngaarden, E., Bosschers, J., Kuiper, G. (2007). “Achievements and challenges in cavitation research on ship propellers.” International Shipbuilding Progress. 54. 2-3.
18. Bosschers, J. (2008) "Analysis of inertial waves on inviscid cavitating vortices in relation to low frequency radiated noise." In Proceedings of the Warwick Innovative Manufacturing Research Centre (WIMRC) Cavitation: Turbo-machinery and Medical Applications Forum. Warwick University.
19. Bosschers, J., (2018) “A Semi-Empirical Prediction Method for Broadband Hull Pressure Fluctuations and Underwater Radiated Noise by Propeller Tip Vortex Cavitation.”, Journal of Marine Science and Engineering. 6. 49. 10.3390/jmse6020049.
20. Pennings, P., Bosschers, J., Westerweel, J., & Van Terwisga, T. (2015), “Dynamics of isolated vortex cavitation.” Journal of Fluid Mechanics, 778, 288-313. doi:10.1017/jfm.2015.379
21. Ceccio, S.L. and Brennen, C.E. (1991), “Observations of the dynamics and acoustics of travelling bubble cavitation.”, J. Fluid Mech., 233, 633–660.

View publication stats